A GATE/Geant4 beam model for the MedAustron non-isocentric proton treatment plans quality assurance

Alessio Elia, Andreas Franz Resch, Antonio Carlino, Till Tobias Böhlen, Hermann Fuchs, Hugo Palmans, Virgile Letellier, Ralf Dreindl, Jhonnatan Osorio, Markus Stock, et al.

Title: A GATE/Geant4 beam model for the MedAustron non-isocentric proton treatment plans quality assurance

Authors: *Alessio Elia*[1], *Andreas Franz Resch*[3,4], *Antonio Carlino*[1], *Till Tobias Böhlen*[1,*], *Hermann Fuchs*[1,3,4], *Hugo Palmans*[1,5], *Virgile Letellier*[1], *Dreindl Ralf*[1], *Osorio Jhonnatan*[1], *Markus Stock*[1], *David Sarrut*[2], *Loïc Grevillot*[1]

[*] *Now with: Paul Scherrer Institut, CH-5232 Villigen PSI, Switzerland.*

Affiliations:

[1] *EBG MedAustron GmbH, Marie-Curie Straße 5, 2700 Wiener Neustadt, Austria e*

[2] *Université de Lyon, CREATIS; CNRS UMR5220; Inserm U1044; INSA-Lyon; Université Lyon 1; Centre Léon Bérard, France.*

[3] *Christian Doppler Laboratory for Medical Radiation Research for Radiation Oncology, Wahringer Guertel 18-20, Medical University of Vienna, Austria*

[4] *Department of Radiation Oncology, Division Medical Physics, Medical University Vienna, Waehringer Guertel 18-20, 1090 Vienna, Austria*

[5] *National Physical Laboratory, Teddington TW 11 0LW, United Kingdom*

E-Mail address:

alessio.elia@medaustron.at

Abstract:

Purpose: to present a reference Monte Carlo (MC) beam model developed in GATE/Geant4 for the MedAustron fixed beam line. The proposed model includes an absolute dose calibration in Dose-Area-Product (DAP) and it has been validated within clinical tolerances for non-isocentric treatments as routinely performed at MedAustron.

Material and Methods: the proton beam model was parametrized at the nozzle entrance considering optic and energy properties of the pencil beam. The calibration in terms of absorbed dose to water was performed exploiting the relationship between number of particles and DAP by mean of a recent formalism. Typical longitudinal dose distribution parameters (range, distal penumbra and modulation) and transverse dose distribution parameters (spot sizes, field sizes and lateral penumbra) were evaluated. The model was validated in water, considering regular-shaped dose distribution as well as clinical plans delivered in non-isocentric conditions.

Results: simulated parameters agree with measurements within the clinical requirements at different air gaps. The agreement of distal and longitudinal dose distribution parameters is mostly better than 1 mm. The dose difference in reference conditions and for 3D dose delivery in water is within 0.5% and 1.2%, respectively. Clinical plans were reproduced within 3%.

Conclusion: a full nozzle beam model for active scanning proton pencil beam is described using GATE/Geant4. Absolute dose calibration based on DAP formalism was implemented. The beam model is fully validated in water over a wide range of clinical scenarios and will be inserted as a reference tool for research and for independent dose calculation in the clinical routine.

Keywords:

GATE/Geant4; proton scanned beam delivery; Monte Carlo; beam modelling; non-isocentric treatment;

1. Introduction

For proton beam delivery, the air gap between the treatment head window (nozzle exit window) and the patient can enlarge the lateral penumbra, as well as lead to lower accuracy of the pencil beam algorithm, especially if the Range Shifter (RaShi) is considered (Soukup *et al* 2005, Saini *et al* 2017). One possible solution to reduce the air gap in clinical practice is to move the patient towards the nozzle exit.

Monte Carlo (MC) simulation tools are often used for independent dose calculation as they can provide useful insights that cannot be obtained otherwise (Tourovosky *et al* 2005, Paganetti *et al* 2008, Perl *et al* 2012, Grevillot *et al* 2012, Magro *et al* 2015). However, any independent dose calculation engine should be carefully characterized and validated before its implementation in clinical applications. Typical characterization of a proton beam can be performed based on measured depth dose curves, spot maps measured at different air gaps and dose measurements in reference condition (Parodi *et al* 2012, Clasie *et al* 2012, Grassberger *et al* 2014). In the literature, different methods for proton pencil beam modeling have been proposed depending on the types of the MC code and on the characteristics of the beam line (Paganetti *et al* 2008, Grassberger *et al* 2014, Grevillot *et al* 2011, Testa *et al* 2013, Fracchiolla *et al* 2015).

For active scanning systems, accurate simulations of a proton pencil beam require a deep understanding of the pencil beam optics properties as the correlation between proton position and angular spread (beam emittance) cannot be neglected a priori (Paganetti *et al* 2008). Omitting the simulation of the nozzle geometry allows an empirical modeling of the pencil beam with an additional reward in computational time (Grassberger *et al* 2014, Grevillot *et al* 2011, Fracchiolla *et al* 2015). Nevertheless, such approach may require additional corrections (Soukup *et al* 2005, Schwaab *et al* 2011) to account for large-angle single scattered primary and secondary particles produced in the nozzle components (Grassberger *et al* 2014, Pedroni *et al* 2005, Sawakuchi *et al* 2010).

In this work, we provide a beam model of the MedAustron fixed beam lines using a full nozzle modeling approach that will be used as a reference for future independent dose calculation. Particular attention is given for the first time to the modeling and to the validation of the pencil beam properties in non-isocentric conditions as routinely exploited for patients treatments at MedAustron since December 2016. In addition, we exploit the Dose-Area-Product (DAP) formalism for absolute dose calibration in terms of delivered protons, differently from the traditional Monitor Unit (MU) calibration (Fracchiolla *et al* 2015, Paganetti *et al* 2006, Mirandola *et al* 2015). The three-dimensional dose distribution simulated in water is carefully validated in terms of ranges, distal penumbra, modulation, field sizes and lateral penumbra, evaluated for different cubic targets in water, including non-isocentric conditions and the use of a range shifter (RaShi). Clinical plans are recalculated in GATE/Geant4 and compared to patient specific quality assurance data.

2. Materials and Methods

2.A. Beam Delivery System

The synchrotron-based Beam Delivery System (BDS) at MedAustron is, in clinical mode, configured to deliver protons at 255 different energies in a range between 62.4 and 252.7 MeV (range in water from 3 to 38 cm in 1 mm steps till 18.8 cm and 2 mm steps otherwise) (Stock *et al* 2017). Using the *slow extraction* method (Bryant *et al* 2000), the particles are extracted from the synchrotron spill by spill and are guided by the High Energy Beam Transport (HEBT) line towards the Irradiation Room (IR) (spill length from 1 s to 5 s). The maximum number of particles extracted per spill is 2E10. A quasi-discrete spot scanning technique has been implemented for active delivery (Haberer *et al* 1993). The nozzle geometry is shown in figure 1. The Water Equivalent Thickness (WET) of the full nozzle is 2.4 mm. Material composition and dimensions of each nozzle element were adopted from the manufacturer or measured wherever possible.

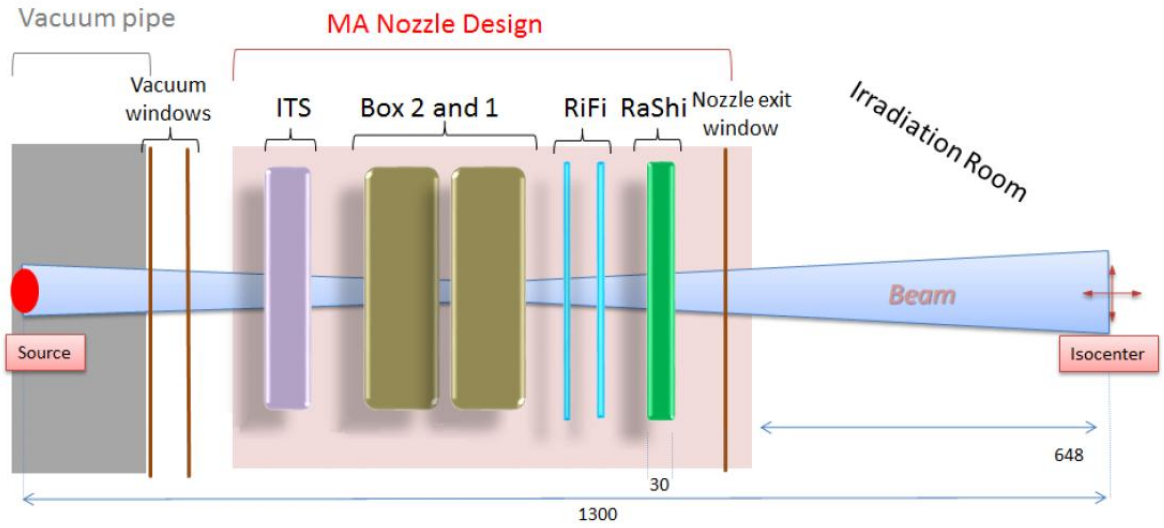

Figure 1: Schematic illustration of the MedAustron (MA) nozzle for the horizontal fixed beam line. It contains a double foil vacuum window, the Independent Termination System (ITS) box, Dose Delivery System (DDS) boxes, and the nozzle exit window. The passive elements, two Ripple Filters (RiFis) and the Range Shifter (RaShi) are also shown. Distances are reported in mm.

2.B. Experimental Data

Experimental data used for beam modeling were acquired during medical physics commissioning of the horizontal beam line (HBL) in the irradiation room 3 (IR3). The Full Width at Half Maximum (FWHM) was extracted from two dimensional lateral dose profiles measured with a scintillating screen detector (Lynx, IBA-dosimetry, Germany) oriented perpendicular to the beam axis.). Spot maps of 9 or 25 regularly spaced spots were delivered over a 20x20 cm2 field size. FWHM were averaged over the entire spot map and were determined at seven isocenter to detector distances (ISD) ranging from +20 cm to -58 cm, which is referred to as ISD+20 and ISD-58, respectively. This corresponds to air-gaps between the nozzle exit and the detector surface ranging from 84.8 cm to 6.8 cm. The air-gap at the isocenter (ISD0cm) is 64.8 cm. The uncertainties on the spot size and position measurements were 0.2 mm (Grevillot *et al* 2018).

Integrated Radial Profiles as function of Depth (IRPDs) were acquired in water using the water phantom MP3-PL (PTW, Freiburg) and the Bragg peak chamber TM 34070 (electrode diameter of 81.6±0.2 mm). The uncertainties of the measured range in water were varying from 0.2 mm to 0.6 mm, depending on the depth and were reproduced with a maximum difference of 0.3 mm (Grevillot *et al* 2018).

For beam monitor calibration in reference condition, absorbed dose to water was measured with a plane parallel ionization chamber (ROOS, TM34001, PTW) in a uniform single-layer of 12x12 cm^2 following IAEA TRS-398 adapted for scanned ion beams (Palmans and Vatnitsky 2016). Dose was measured at 1.4 cm depth in water for energies up to 97.4 MeV and at 2.0 cm depth for larger energies, up to 252.7 MeV. DAP to water was derived by multiplying the absorbed dose to water with the product of the constant spot spacing Δx Δy as described in Palmans and Vatnitsky (Palmans and Vatnitsky 2016).

The dose was measured at several positions in clinical treatment plans in order to validate the combined beam model. To minimize volume averaging effects, 24 of the smallest available ICs were used in the MP3-PL water phantom (PinPoint TM 31015, volume 0.03 cm^3 and radius 1.45 mm, PTW, Freiburg) characterized in photons and proton beams (Carlino *et al* 2018). The 24 PinPoints were mounted in a special holder (3D Detector Block) such that they do not shield each other in beam's eye view. The same setup was used to measure clinical plans. Table 1 summarizes the measurements performed and their purposes.

Purpose	Measurement description	Measured quantity	Measured data set
Beam optics modeling	spot map	Source Axes Distance, FWHM in air	20 energies per 7 air gaps
Energy spectra modeling	depth dose profile for a pristine Bragg curve	range in water, integrated depth dose profile	20 energies at isocenter
Beam optics residual evaluation with RaShi	spot map	FWHM in air	4 energies, 5 air gaps, with RaShi
Depth dose residual evaluation with RaShi	depth dose profile single spot	range in water, integrated depth dose profile	4 energies measured at non-isocentric position with RaShi
Beam model dose calibration and residual evaluation in 2D	dose in reference condition for scanned fields	Dose Area Product	9 energies
Beam model final validation in 3D	3D dose distribution in water	field size, lateral penumbra, modulation, dose	3 boxes measured at isocenter, 1 non-isocentric box with RaShi, 7 clinical plans in non-isocentric conditions with or without RaShi

Table 1: Summary of experimental data used for generation of the MC beam model and for its validation.

2.C. MC beam modeling

All MC simulations were performed including the full nozzle geometry. The MC beam model was developed consecutively. Starting with a preliminary energy tuning using the nominal beam energy. Subsequently, the pencil beam optical properties were fine-tuned and the energy and energy spread

were fine-tuned using the measured IRPDs. Finally, the MC simulations were exploited to retrieved the delivered number of particles per spot from the measured DAP. MC beam parameters were optimized for a subset of different energies and a polynomial interpolation was applied for the intermediate energies.

GATE v7.2 (Sarrut *et al* 2014, Jan *et al* 2011) built with Geant4 v10.02 (Allison *et al* 2006, Allison *et al* 2016) was used to carry out the MC simulations. The QBBC_EMZ physics builder (Ivantchenko *et al* 2012) was selected (Resch *et al* 2019). A constant maximum step limiter, tracking cut and range cut were set equal to 0.1 mm was applied (Grevillot *et al* 2010). The mean excitation energy of water I_w was set to 78 eV following the recommendations in ICRU Report 90 (ICRU report 90 2014). For the beam optics modeling and the IRPDs simulations, 1E5 and 1E6 primaries were simulated.

Beam optic properties

The FWHMs were extracted from the particles phase space using the Gate *PhaseSpaceActor* attached to planes corresponding to the measured ISDs. A straight pencil beam was considered in our simulation to initially model the optic properties. The beam optics parameters were iteratively adapted to minimize the differences between measured and simulated FWHM at all ISDs for the horizontal and for the vertical plane independently. The tolerance level was defined as 1 mm in absolute deviation or 10% in relative deviation according to clinical practice at MedAustron.

IRDPs

IRPDs were scored in a water cylindrical geometry mimicking the active volume of the Bragg chamber (radius 40.8 mm). The maximum resolution of the measurements was used as MC scoring resolution (0.1 mm) (Grevillot et al 2018). Parameters of the MC simulations being tuned were the mean energy E and the energy spread ΔE. Energy properties were estimated by an iterative procedure to match MC simulations with measurements in terms of physical range (R80) and Bragg peak width at the 80% dose level (BPW80). Other parameters were evaluated: clinical range (R90) and practical range (Rp) defined as the 90% and 10% dose level, respectively, in the distal fall-off of a depth dose profile.

Beam model calibration

One possibility to calibrate a MC beam model in absolute dose is to establish the relationship between the delivered number of particles N and DAP in reference conditions (Palmans and Vatnitsky 2016):

$$\mathrm{N}_{\mathrm{delivered}} = \frac{DAP_w^A(z_{ref})}{d_w(S_{el}^{\rho}, \Phi_z^A) \cdot A} \quad (1)$$

The numerator of the equation 1 is the experimentally determined DAP in water at the reference depth z_{ref} over the area *A*. In general, the term $d_w(S_{el}^{\rho}, \Phi_z^A)$ represents the "mean stopping power" per incident proton evaluated in water by any dose engine and it is characterized as follow:

$$d_w(S_{el}^{\rho}, \Phi_z^A) = \frac{\sum_i \int (S_{el,i}/\rho)_w \, \Phi_{E,i}^A(z_{ref}) dE}{n} \quad (2)$$

In the expression 2, $(S_{el,i}/\rho)_w$ is the mass electronic stopping power of water for ion species *i* and $\Phi_{E,i}^{A}(z_{ref})$ is the fluence differential in energy of that ion species at the reference depth z_{ref} (Palmans and Vatnitsky 2016). The key point of this approach is to calculate by a MC simulation the $d_w(S_{el}^{\rho}, \Phi_z^A)$ term for a known number of protons *n*, as described by equation 2. Therefore, a single pencil beam was simulated and scored in a cylindrical volume of 7 cm radius, sufficiently large to encompass all the charged particles of the radiation field over the full clinical energy range. Electrons were not tracked by applying a production cut of 5 mm meaning that electrons with a CSDA range lower than 5 mm in the current medium are not transported in the simulation; their energy is considered deposited locally. Depending on the energy, two reference depths were considered: 1.4 cm in the energy range between 62.4 MeV and 97.4 MeV, and 2 cm from 97.4 MeV up to the maximum energy (252.7 MeV) (see section 2.B). Mean stopping power values computed with GATE were used during medical commissioning of the MedAustron beam delivery system in order to calibrate the beam monitors in number of particles per MU (N/MU). Hence, measured DAP and simulated DAP should be in perfect agreement.

2.D. Beam model validation

Regular shaped targets in water

The beam model was validated by means of 3D dose distributions in water for four regular shaped dose cubes of different dimensions and depths in water, following a similar methodology as for the commissioning of the Treatment Planning System (TPS) (Carlino *et al* 2019). The so-called Box6(0,0,6), Box8(0,0,15), and Box10(0,0,25) were delivered at isocenter where the notation BoxN(0,0,Z) stands for a cubic dose distribution with an N cm side-length and its center placed at the water equivalent depth Z. The Box6(0,0,5), was delivered in non-isocentric conditions (ISD-50cm) using a RaShi. Each treatment plan (TP) was simulated using 1.8E8 primaries. The average unsigned and signed local dose deviations were evaluated:

$$\bar{\Delta} = \frac{1}{K}\sum_{i}^{K} \frac{D_i^{GATE} - D_i^{meas}}{D_i^{meas}} \quad (3)$$

$$\bar{\Delta}_{ABS} = \frac{1}{K}\sum_{i}^{K} \frac{|\, D_i^{GATE} - D_i^{meas} \,|}{D_i^{meas}} \quad (4)$$

where K is the number of PinPoint ICs used in the measurements, D_i^{meas} the dose measured for the chamber *i* and D_i^{GATE} the calculated dose. For the evaluation of $\bar{\Delta}$ and $\bar{\Delta}_{ABS}$, the 3D holder was placed in a region were at least 95% of the prescribed dose (1 Gy) was reached (target region). Wherever possible, an additional evaluation was performed for the plateau dose region (proximal region), where a dose level within 60% and 95% of the prescribed dose was reached. IC measurements located at a local dose gradient higher than 0.04 Gy/mm were excluded from the analysis as small positioning and range uncertainties or volume averaging effects would cause high deviations (Magro *et al* 2015, Carlino 2017, Resch *et al* 2019). Transverse dose profiles were selected at the center of the SOBP and analysed in terms of Field Size at 50% (FS50) and Lateral Penumbra between 80% and 20% (LP80-20) of the dose profile. Furthermore, distal parameters such as R90,

R80, Rp, SOBP modulation defined at 90% dose level (MOD90) and distal penumbra between 80% and 20% dose levels (DP80-20) were analysed.

Clinical TP scenarios

For clinical validation, the patient specific quality assurance (PSQA) of seven patients were selected (33 beams in total). The clinical indications were: two clivus chordoma of the brain, a carcinoma of the palate (para-nasal case), a prostate carcinoma, an adenoid cystic carcinoma (head and neck case), a nasopharyngeal carcinoma and a skull-base meningioma. The Planning Target Volume (PTV) ranged from 21.56 up to 302.16 cm^3 located at depths from approximately 3 cm (proximal) to 22 cm (distal) for the non-RaShi fields. Three RaShi beams were included in the evaluation. Each beam was measured up to three different position with 24 PinPoint ICs. In contrast to the regular shaped targets, the planned dose level varied considerably in the beams of the irregular shaped targets. To account for the varying dose level, a relative dose gradient threshold equal to 2%/mm was applied. A total of 1344 dose measurement points were evaluated. In average, 15 points per beam were passing the dose gradient threshold. All the PSQA plans were measured in non-isocentric conditions at ISD-40cm, following the methodology reported in Carlino 2017 (Carlino 2017).

3. Results and Discussion

3.A. Beam modeling accuracy

Beam optics properties

The optical beam model parameters found resulted in a 99% pass rate of the FWHM using the clinical 1mm/10% requirement over the entire 86 cm air-gap range. The largest deviations of 1.8 mm (7.2%) and 1.7 mm (6.9%) were obtained for 62.4MeV at ISD+20cm in the vertical and horizontal planes, respectively. The accuracy of the multiple Coulomb scattering model implemented in Geant4 is mainly driving the agreement in FWHM as the scattering in air is the most predominant effect for this energy and position. However, this combination of energy and position is not clinically relevant in proton therapy. With RaShi the residuals in FWHM were systematically shifted in positive direction (see figure 2). This may be due to the multiple Coulomb Scattering uncertainties in the RaShi (PMMA) (Fuchs *et al* 2017, Resch *et al* 2018). However, observed deviations were still within clinical tolerances.

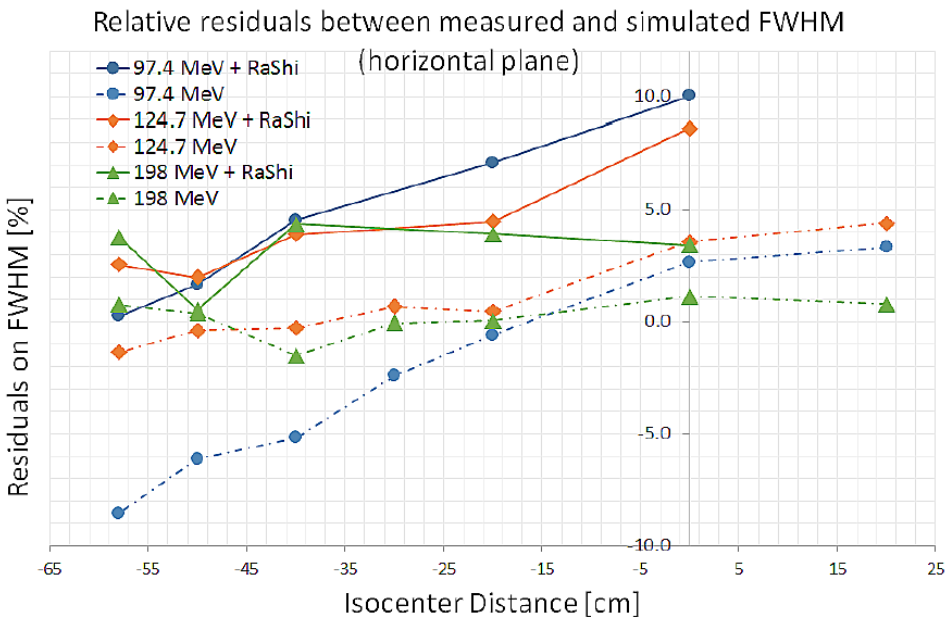

Figure 2: FWHM agreement in relative terms between simulated and measured values with and without RaShi for the horizontal plane. For clarity purpose, only three representative energies are shown. Similar results were obtained for the vertical plane.

IRDPs

All 20 measured and simulated IRPDs are shown in figure 3(a).

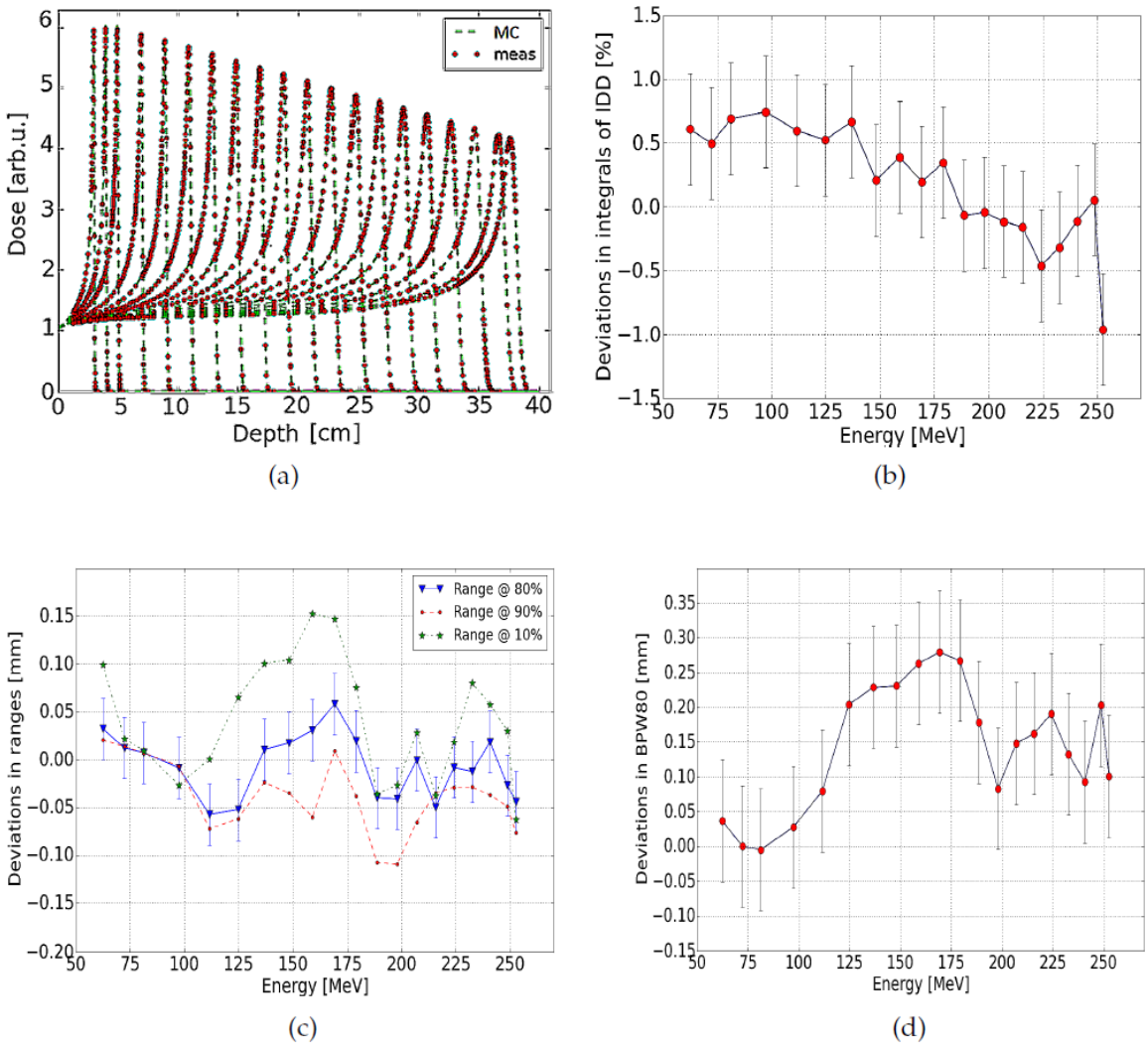

Figure 3: In figure 3(a) depth dose profiles simulated in water compared to measured profiles for 20 energies are shown. For this comparison, energy values deposited in the cylindrical volume representing the Bragg peak chamber of 4.08 cm radius was used. In figure 3(b) relative deviations between simulated and measured integral doses are shown. In figure 3(c) absolute deviations between simulated and measured ranges are shown while in figure 3(d) absolute deviations of Bragg peak width values at 80% dose level are reported. Error bars always correspond to the standard deviation. For sake of clarity, in figure 3(c) error bars are reported for only one set of deviations.

The integrals of the measured and simulated IRPDs normalized at the first measurement point agreed within 1% (see figure 3(b)) in the entire energy range. Simulated ranges deviated less than 0.2 mm with measurements as can be seen in figure 3(c). The BPW80 deviated by 0.1 mm on average which corresponds to a relative deviation of about 3% (see figure 3(d)). Maximum absolute deviation was 0.3 mm (6%) at 169.3 MeV. Deviations of R80, R90 and Rp for depth dose profiles in water at ISD-50cm with RaShi were less than 0.3 mm while mean integral dose deviations as well as the average peak-to-plateau differences were better than 0.4%.

Beam model calibration

We present in table 2 the differences between our calculated “mean stopping power” (full MC simulation) and ICRU stopping power data (mono-energy beam) for protons with the same residual range at the measurement depth. Differences up to 10.4% were found, with an expected energy dependent behavior. Indeed, ICRU stopping power data are provided for mono-energetic pencil

beams, while the "mean stopping power" accounts for the loss of primary protons but includes the nuclear secondaries at the measurement depth. This result illustrates the importance of taking the loss of primary protons and the production of secondary charged particle into account.

z_{ref} [cm]	Nominal energy [MeV/n]	Monte Carlo $d_w(S_{el}^{\rho}, \Phi_z^A)$ [MeV cm^2 g^{-1}]	R80 [cm]	Rp [cm]	R80-z_{ref} [cm]	ICRU90 $(S/\rho)_w(E_i, z_{ref})$ [MeV cm^2 g^{-1}]	relative difference to ICRU90 [%]
1.4	62.4	14.48	2.98	3.11	1.58	14.42	0.39%
1.4	72.4	11.80	3.98	4.12	2.58	11.63	1.47%
1.4	81.3	10.29	4.98	5.12	3.58	10.08	2.13%
1.4	97.4	8.55	6.98	7.14	5.58	8.34	2.57%
2.0	97.4	8.99	6.98	7.14	4.98	8.75	2.71%
2.0	111.6	7.86	8.97	9.18	6.97	7.59	3.64%
2.0	124.7	7.12	10.99	11.23	8.99	6.82	4.30%
2.0	136.8	6.60	12.99	13.27	10.99	6.28	5.35%
2.0	148.2	6.21	15.00	15.31	13.00	5.86	5.78%
2.0	159.0	5.88	17.00	17.34	15.00	5.54	6.30%
2.0	169.3	5.64	19.00	19.39	17.00	5.27	7.10%
2.0	179.2	5.42	21.00	21.41	19.00	5.04	7.43%
2.0	188.7	5.23	22.98	23.42	20.98	4.85	7.79%
2.0	198.0	5.07	24.99	25.46	22.99	4.68	8.18%
2.0	207.0	4.93	26.99	27.49	24.99	4.54	8.50%
2.0	215.7	4.81	28.97	29.51	26.97	4.41	8.97%
2.0	224.2	4.69	30.96	31.53	28.96	4.29	9.28%
2.0	232.6	4.58	32.97	33.58	30.97	4.19	9.34%
2.0	240.8	4.50	35.00	35.64	33.00	4.09	10.07%
2.0	248.8	4.41	36.99	37.66	34.99	4.01	10.09%
2.0	252.7	4.37	38.08	38.68	36.08	3.96	10.36%

Table 2: Summary of the "mean stopping power" calculated according to equation 2. The energy is provided at the nozzle entrance. The last two columns shows the ICRU90 stopping power for mono-energetic protons with the same residual range and the difference of those values from the "mean stopping power" per incident proton.

Our results are in agreement with previous publications (Laitano *et al* 2000, Gomá *et al* 2016). The number of incident proton at nozzle entrance is used to normalized the DAP values. In our simulations, less than 1.0% and 0.5% proton loss was found at the phantom entrance and at the nozzle exit, respectively. The contribution of the nozzle to the primary fluence loss is in agreement with the 0.58% reported by Grassberger et al. (Grassberger *et al* 2014).

Agreement in terms of DAP is shown in figure 4. A mean agreement of -0.1% between simulated and measured DAP was found and maximum deviation was -0.5% at 62.4 MeV. The comparison to measured DAP is an internal consistency test of the correct implementation of the MC calculated values of the "mean stopping power" per incident proton for beam monitor calibration. The residuals shown in figure 4 are the result of the fitting of the calibration curve as we have observed before.

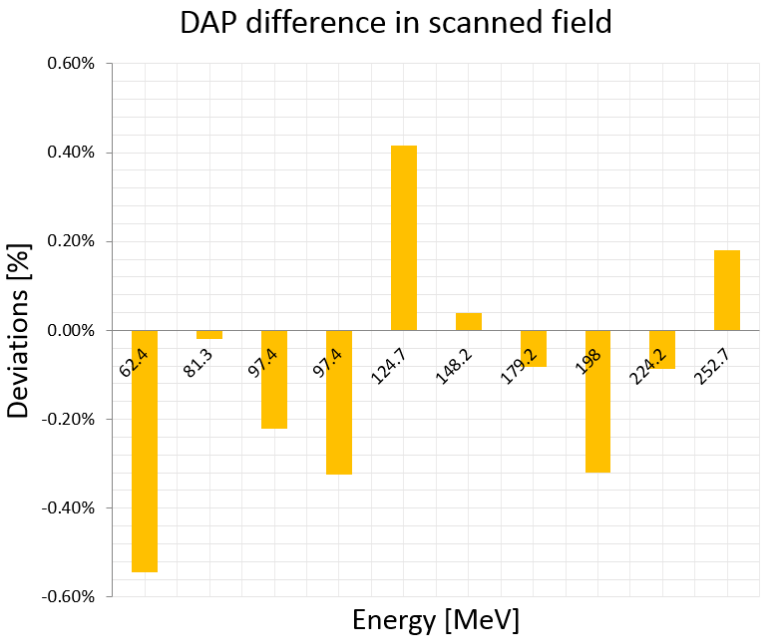

Figure 4: Relative deviations in terms of DAP per incident proton for a 2D scanned field 12x12 cm^2 and measured at the reference position of 1.4 and 2 cm in depth (depending on the energy).

3.B. Beam model validation

Regular shaped targets in water

The transverse and longitudinal dose distribution parameters were in satisfactory agreement with measurements and are summarized in table 3. The FS50 and the LP80-20 agreed on average by 0.4 mm and -0.1 mm, respectively. For the FS50, a maximum deviation of -1.0 mm (-11.4% in relative terms) was observed for the shallower target (95% dose level within 3 and 8 cm range) when the RaShi was used. Deviations for R80 and R90, initially found never higher than 0.2 mm, increase up to 0.5 mm and 0.7 mm, respectively, when a RaShi was used. A spread of 1.3 mm was found in the evaluation of the MOD90 over all the boxes, with a maximum deviation of 2.1 mm for the deepest target (95% dose level within 22 and 30 cm range). The DP80-20 was -0.3 mm in average with a maximum deviation of -0.6 mm.

The averaged signed dose deviated on average over all measured points in the regular shaped targets by +2.7%. This dose difference was found consistent for all boxes and independent of the position (proximal or SOBP), air gap, box size and use of range shifter. The reason for the systematic difference of about 2.7% initially observed in the 3D delivery is currently not understood and is still under investigation. A similar off-set in the same direction was also found during the validation of the beam model implemented in the RayStation TPS (RaySearch Laboratories (RSL), Sweden) as reported by Carlino et al. (Carlino *et al* 2019). Several factors from the absolute dosimetry to the beam modeling process itself can add up and lead to a systematic offset. One of the main contributions could be imprecisions in the description of the shape of the pre-defined mono-energetic Bragg peaks to fit the experimental IRPDS provided by the clinic. The shape of the pre-defined mono-energetic Bragg peaks depends substantially on the choice of the MC code and physics settings (mainly the hadronic models and the nuclear cross sections (Grevillot *et al* 2010, Resch *et al* 2019) and the deficiency of the fitting

process may cause the off-set. Therefore, the absolute dose calibration was rescaled by -2.7%. After rescaling, the largest deviation was -1.2% at the proximal position for the Box10 (see figure 5).

Box type	FS50 [mm]	LP80-20- [mm]	LP80-20+ [mm]
Box6(0,0,6)	0.3 (0.4%)	-1.0 (-11.4%)	0.0 (0.1%)
Box8(0,0,15)	0.3 (0.3%)	-0.2 (-2.4%)	-0.2 (-2.0%)
Box10(0,0,25)	0.1 (0.1%)	0.3 (1.1%)	0.2 (2.1%)
Box6(0,0,5) ISD-50cm+RaShi	1.0 (1.2%)	-0.4 (10.3%)	0.2 (-2.4%)

Box type	R80 [mm] (%)	R90 [mm] (%)	Rp [mm] (%)	MOD90 [mm] (%)	DP80-20 [mm] (%)
Box6(0,0,6)	0.0 (0.0%)	0.1 (0.0%)	-0.7 (-0.7%)	-1.0 (-1.5%)	-0.6 (-24.7%)
Box8(0,0,15)	0.0 (0.0%)	0.0 (0.0%)	-0.4 (-0.2%)	1.3 (1.4%)	-0.5 (-14.0%)
Box10(0,0,25)	-0.1 (0.0%)	-0.2 (-0.1%)	-0.4 (-0.1%)	2.1 (1.7%)	-0.5 (-9.0%)
Box6(0,0,5) ISD-50cm+RaShi	0.5 (0.6%)	0.7 (0.9%)	-0.2 (-0.2%)	0.8 (1.3%)	-0.5 (-16.0%)

Table 3: Deviations in water for the 3D dose distributions analysed in terms of transverse dose distribution parameters (above) and distal dose distribution parameters (below) in absolute and relative terms. The LP80-20- and the LP80-20+ are referring to the LP80-20 evaluated for the negative and the positive distance, respectively, from the center of the transverse dose profile.

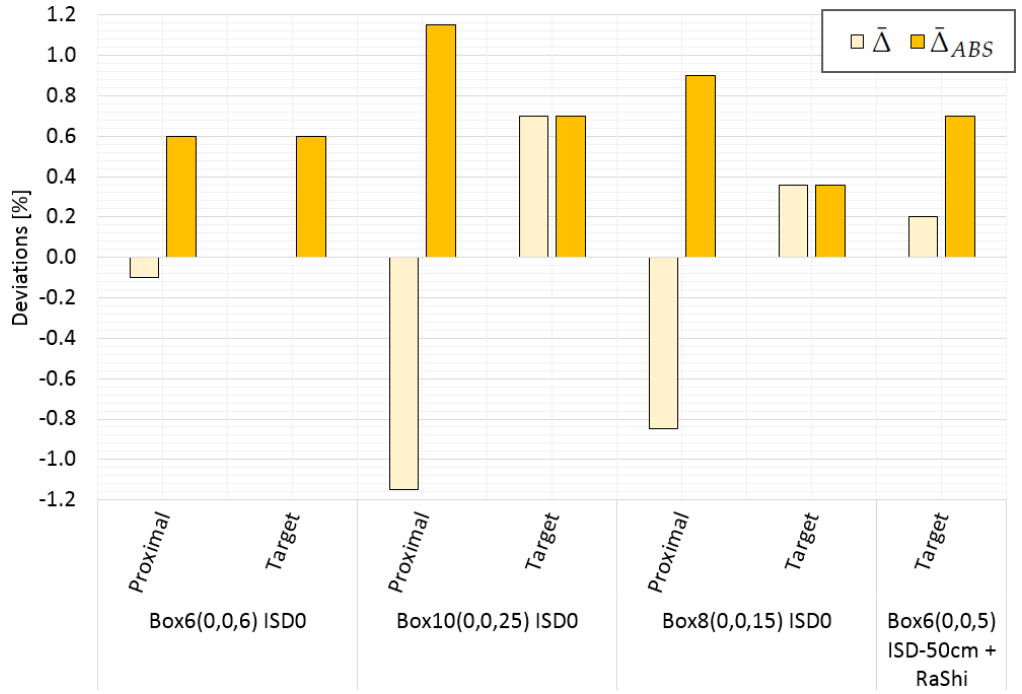

Figure 5: Local dose deviations evaluated according to equation 3 and equation 4 after rescaling of -2.7%.

The target dose in the regular shaped dose distributions was accurate to within +/- 1.0% in isocentric as well as non-isocentric conditions (varying air gaps and the use of the RaShi). A maximum average deviation of -0.2% was found in the SOBP for the non-isocentric Box6 with RaShi. All the analyzed regular shaped targets in water are shown in figure 6 and figure 7. The presented analysis suggest the

tendency of an underestimation of the dose in the plateau by about -1% and an overestimation towards the end of the SOBP by about +1%.

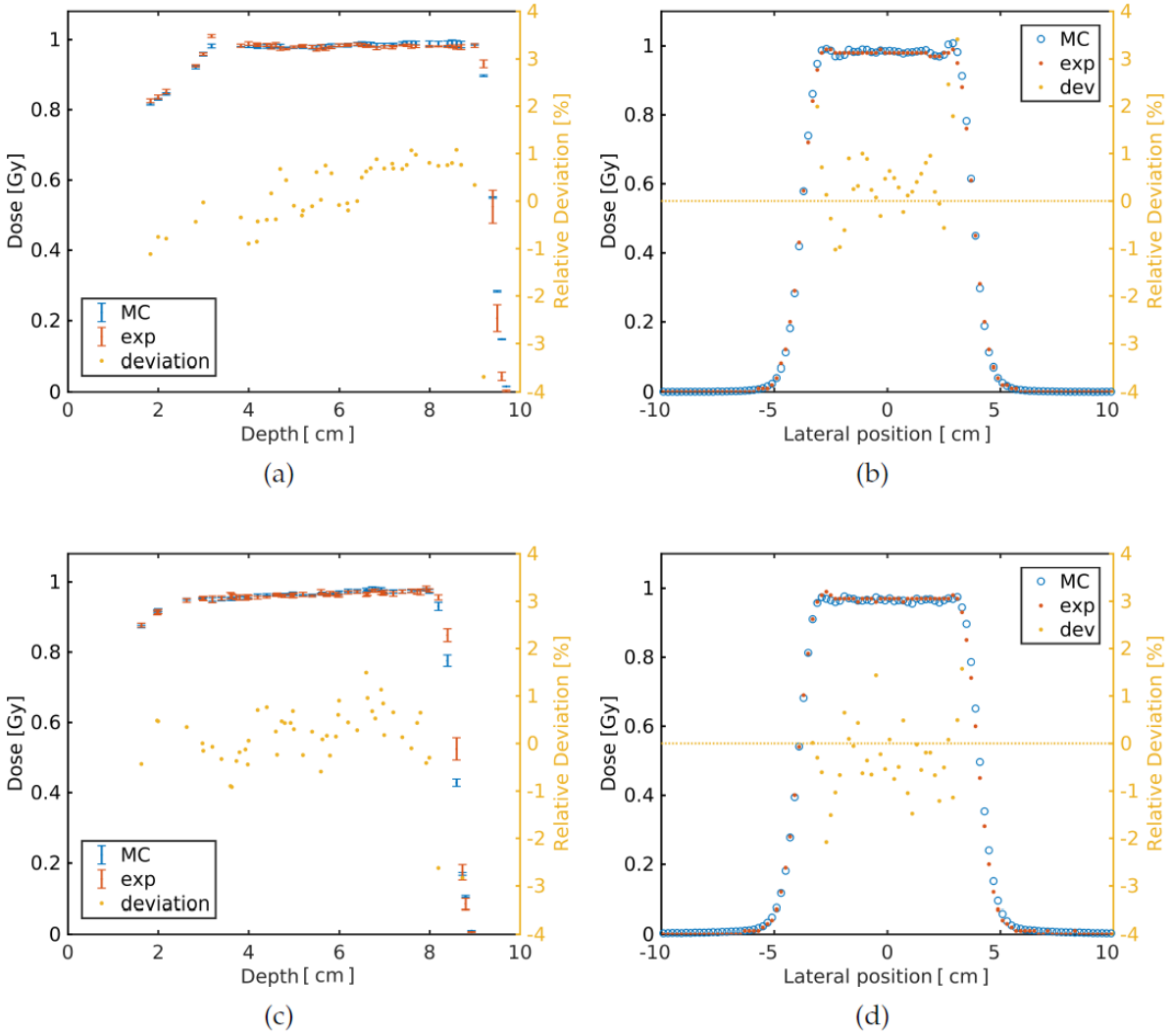

Figure 6: Longitudinal (a) and transverse (b) dose profiles for Box6(0,0,6) and longitudinal (c) and transverse (d) dose profiles for the Box6(0,0,5) placed at ISD-50cm with RaShi compared to measurements.

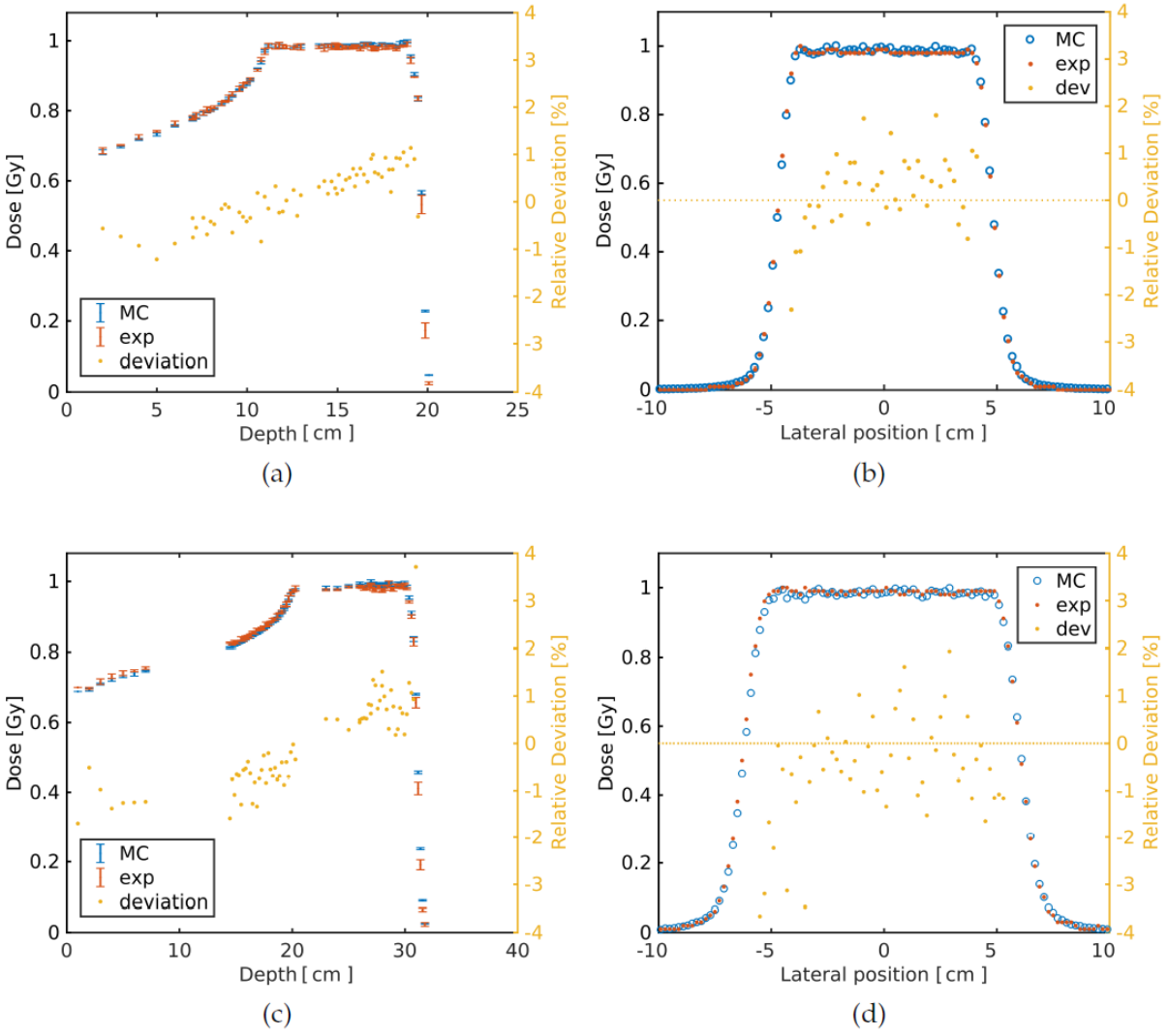

Figure 7: Longitudinal (a) and transverse (b) dose profiles for Box8(0,0,15) and longitudinal (c) and transverse (d) dose profiles for the Box10(0,0,25) compared to measurements.

Clinical TP scenarios

The dose differences in the clinical treatment plans at ISD-40cm were negligible at low dose gradients, whereas up to 3% deviations were found at high dose gradients. Almost zero deviation and a low standard deviation was found where the average local dose gradient at the measurement points was less than 1 %/mm (see figure 8). Fluctuations and standard deviation increased for higher dose gradient indicating a sensitivity to positioning uncertainty. The three beams with RaShi showed a tendency of underestimating the dose, but the significance of those findings is limited due to the high dose gradient at the measurement points which was 1.2 %/mm on average. The RaShi is required to cover targets shallower than 3 cm, which is difficult to measure with the 24 PinPoints system.

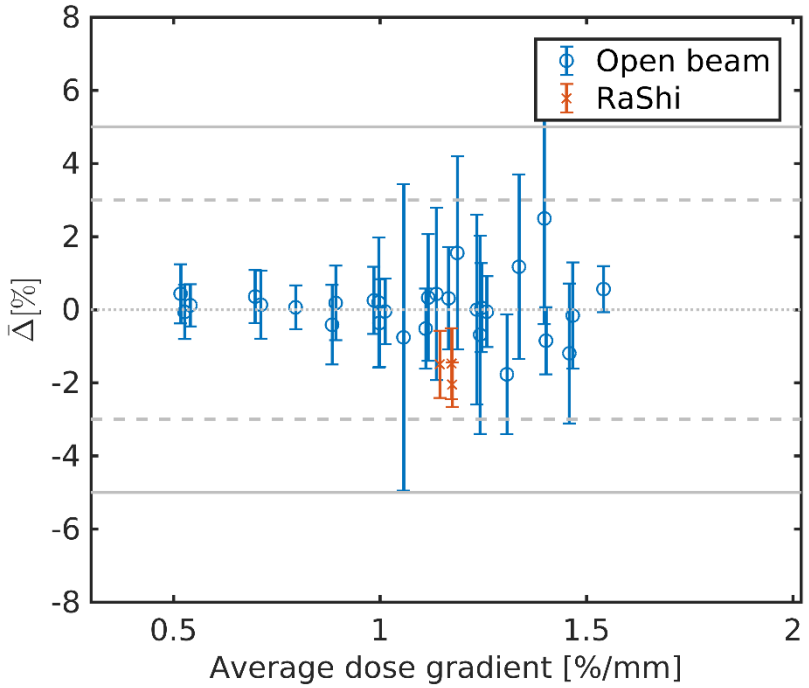

Figure 8: Local average dose deviation per beam in clinical cases as a function of the averaged dose gradient. Error bars represents the standard deviation of the relative deviations. The 3% and 5% level are indicated with dashed and solid lines, respectively.

Conclusion

A full nozzle beam model for scanned proton beam delivery has been validated with GATE/Geant4. This beam model starts at nozzle entrance tracking all particles through the nozzle elements, which allows to account for physical interactions within the treatment head, including the passive elements.

The beam model was validated in isocentric and non-isocentric treatment conditions, as routinely performed at MedAustron since 2016. The beam spot size evaluated in FWHM in vertical and horizontal direction fulfilled clinical requirements of 1 mm and 10% at seven positions ranging over 86 cm of air gap. Ranges were reproduced within 0.2 and 0.3 mm (max deviation) without and with range shifter, respectively.

The calibration of the beam monitors is based on a new formalism in dose-area-product and has been clinically implemented for the first time.

Three-dimensional delivery was benchmarked using commissioning data and clinical PSQA measurements. Typical parameters such as field size, modulation, lateral and distal penumbra and range were well reproduced. The dose in the 3D regular shaped targets showed a systematic deviation of +2.7% on average, independently of the treatment depth, field size and modulation. Therefore a final rescaling factor of 0.973 was applied to the beam model and used as such in the rest of the work. The reasons for this deviation are currently unclear and will be the subject of further studies.

Final validation of the beam model using clinical TP scenarios agreed within 1% when the average dose gradient at the measurement positions was less than 1 %/mm.

The detailed characterization of the pencil beam offered by GATE and the implementations of the full nozzle design in our simulations makes our MC beam model accurate, even in complex situations such as the non-isocentric patient positioning in presence of range shifter. The MC beam model will be exploited for future research work and will be inserted as a tool in clinical routine for independent dose calculation in isocentric and non-isocentric conditions.

Acknowledgment

The authors are grateful to all the colleagues at the MedAustron medical physics department (Wiener Neustadt, Austria), in particular to Stanislav Vatnitsky for remarkable discussions. The entire CREATIS group at the Léon Bérard hospital (Lyon, France) is fully acknowledged. This work was performed within the framework of the SIRIC LYriCAN Grant INCa_INSERM_DGOS_12563, and the LABEX PRIMES (ANR-11-LABX-345 0063) of Université de Lyon, within the program ANR- 11-IDEX-0007. The financial support by the (Austrian) Federal Ministry for Digital, Business and Enterprise and the National Foundation for Research, Technology and Development is gratefully acknowledged.

Bibliography

Martin Soukup, Matthias Fippel, and Markus Alber. A pencil beam algorithm for intensity modulated proton therapy derived from monte carlo simulations. *Physics in Medicine & Biology*, **50**(21):5089, 2005.

Jatinder Saini, Dominic Maes, Alexander Egan, Stephen R Bowen, Sara St James, Martin Janson, TonyWong, and Charles Bloch. Dosimetric evaluation of a commercial proton spot scanning Monte-Carlo dose algorithm: comparisons against measurements and simulations. *Physics in Medicine and Biology*, 2017.

A Tourovsky, AJ Lomax, U Schneider, and E Pedroni. Monte carlo dose calculations for spot scanned proton therapy. *Physics in Medicine & Biology*, **50**(5):971, 2005.

Harald Paganetti, Hongyu Jiang, Katia Parodi, Roelf Slopsema, and Martijn Engelsman. Clinical implementation of full monte carlo dose calculation in proton beam therapy. *Physics in Medicine & Biology,* **53**(17):4825, 2008.

Joseph Perl, Jungwook Shin, Jan Schümann, Bruce Faddegon, and Harald Paganetti. Topas: An innovative proton monte carlo platform for research and clinical applications. *Medical physics,* **39**(11):6818–6837, 2012.

L Grevillot, D Bertrand, F Dessy, N Freud, and D Sarrut. GATE as a GEANT4-based Monte Carlo platform for the evaluation of proton pencil beam scanning treatment plans. *Physics in medicine and biology*, **57**(13):4223, 2012.

G Magro, S Molinelli, A Mairani, A Mirandola, D Panizza, S Russo, A Ferrari, F Valvo, P Fossati, and M Ciocca. Dosimetric accuracy of a treatment planning system for actively scanned proton beams and small target volumes: Monte carlo and experimental validation. *Physics in Medicine & Biology,* **60**(17):6865, 2015.

Carlino, Antonio, "Implementation of advance methologies in the commissioning of a Light Ion Beam Therapy facility" *University of Palermo*. PhD dissertation (2017)

Katia Parodi, Andrea Mairani, Stephan Brons, BG Hasch, Florian Sommerer, J Nau mann, Oliver Jäkel, Thomas Haberer, and Jürgen Debus. Monte carlo simulations to support start-up and treatment planning of scanned proton and carbon ion therapy at a synchrotron-based facility. *Physics in medicine and biology*, **57**(12):3759, 2012.

Benjamin Clasie, Nicolas Depauw, Maurice Fransen, Carles Gomà, Hamid Reza Panahandeh, Joao Seco, Jacob B Flanz, and Hanne M Kooy. Golden beam data for proton pencil-beam scanning. *Physics in medicine and biology*, **57**(5):1147, 2012.

C Grassberger, Anthony Lomax, and H Paganetti. Characterizing a proton beam scanning system for Monte Carlo dose calculation in patients. *Physics in medicine and biology*, **60**(2):633, 2014.

L Grevillot, D Bertrand, F Dessy, N Freud, and D Sarrut. A Monte Carlo pencil beam scanning model for proton treatment plan simulation using GATE/GEANT4. *Physics in Medicine and Biology*, **56**(16):5203, 2011.

M Testa, J Schümann, H-M Lu, J Shin, B Faddegon, J Perl, and H Paganetti. Experimental validation of the topas monte carlo system for passive scattering proton therapy. *Medical physics*, **40**(12), 2013.

F Fracchiolla, S Lorentini, LWidesott, andM Schwarz. Characterization and validation of a monte carlo code for independent dose calculation in proton therapy treatments with pencil beam scanning. *Physics in medicine and biology*, **60**(21):8601, 2015.

J Schwaab, Stephan Brons, J Fieres, and Katia Parodi. Experimental characterization of lateral profiles of scanned proton and carbon ion pencil beams for improved beam models in ion therapy treatment planning. *Physics in Medicine & Biology*, **56**(24):7813, 2011.

E Pedroni, S Scheib, T Böhringer, A Coray, M Grossmann, S Lin, and A Lomax. Experimental characterization and physical modelling of the dose distribution of scanned proton pencil beams. *Physics in Medicine & Biology*, 50(3):541, 2005.

Gabriel O Sawakuchi, Uwe Titt, Dragan Mirkovic, George Ciangaru, X Ronald Zhu, Narayan Sahoo, Michael T Gillin, and Radhe Mohan. Monte carlo investigation of the low-dose envelope from scanned proton pencil beams. *Physics in Medicine & Biology*, **55**(3):711, 2010.

Hugo Palmans and Stanislav M Vatnitsky. Beam monitor calibration in scanned light ion beams. *Medical physics*, **43**(11):5835–5847, 2016.

Carlino, Antonio, Till Boehlen, Stanislav Vatnitsky, Loic Grevillot, Jhonnatan Osorio, Ralf Dreindl, Hugo Palmans, Markus Stock, and Gabriele Kragl. "Commissioning of pencil beam and Monte Carlo dose engines for non-isocentric treatments in scanned proton beam therapy." *Physics in Medicine & Biology* (2019).

Harald Paganetti. Monte carlo calculations for absolute dosimetry to determine machine outputs for proton therapy fields. *Physics in Medicine & Biology*, **51**(11):2801, 2006.

Alfredo Mirandola, S Molinelli, G Vilches Freixas, A Mairani, E Gallio, D Panizza, S Russo, M Ciocca, M Donetti, G Magro, et al. Dosimetric commissioning and quality assurance of scanned ion beams at the italian national center for oncological hadron-therapy. *Medical physics*, **42**(9):5287–5300, 2015.

Markus Stock, Dietmar Georg, Alexander Ableitinger, Andrea Zechner, Alexander Utz, Marta Mumot, Gabriele Kragl, Johannes Hopfgartner, Joanna Gora, Till Böhlen, et al. The technological basis for

adaptive ion beam therapy at medaustron: status and outlook. *Zeitschrift für Medizinische Physik*, 2017.

PJ Bryant, L Weisser, L Badano, G Borri, M Crescenti, P Holy, S Reimoser, AT Maier, P Knaus, M Pavlovic, et al. Proton-Ion Medical Machine Study (PIMMS), 2. Technical report, 2000. 22Th Haberer, W Becher, Dieter Schardt, and Gerhard Kraft. *Magnetic scanning system for heavy ion therapy. Nuclear Instruments and Methods in Physics Research Section A: Accelerators, Spectrometers, Detectors and Associated Equipment*, **330**(1-2):296–305, 1993.

Loïc Grevillot, Markus Stock, Hugo Palmans, Jhonnatan Osorio Moreno, Virgile Letellier, Ralf Dreindl, Alessio Elia, Hermann Fuchs, Antonio Carlino, and Stanislav Vatnitsky. Implementation of dosimetry equipment and phantoms at the medaustron light ion beam therapy facility. *Medical physics*, **45**(1):352–369, 2018.

David Sarrut, Manuel Bardiès, Nicolas Boussion, Nicolas Freud, Sébastien Jan, Jean-Michel Létang, George Loudos, Lydia Maigne, Sara Marcatili, Thibault Mauxion, Panagiotis Papadimitroulas, Yann Perrot, Uwe Pietrzyk, Charlotte Robert, Dennis R. Schaart, Dimitris Visvikis, and Irène Buvat. A review of the use and potential of the GATE Monte Carlo simulation code for radiation therapy and dosimetry applications. *Medical Physics*, **41**(6):064301, 2014.

S. Jan, D. Benoit, E. Becheva1, T. Carlier, F. Cassol, P. Descourt, T. Frisson, L. Grevillot, L. Guigues, L. Maigne, C. Morel, Y. Perrot, N. Rehfeld, D. Sarrut, D. R. Schaart, S. Stute, U. Pietrzyk, D. Visvikis, N. Zahra, , and I. Buvat. GATE V6: a major enhancement of the GATE simulation platform enabling modelling of CT and radiotherapy. *Physics in Medicine and Biology,* **56**:881–901, 2011.

John Allison, Katsuya Amako, Jea Apostolakis, HAAH Araujo, P Arce Dubois, MAAM Asai, GABG Barrand, RACR Capra, SACS Chauvie, RACR Chytracek, et al. *Geant4 developments and applications. IEEE Transactions on nuclear science*, **53**(1):270–278, 2006.

J Allison, Katsuya Amako, J Apostolakis, Pedro Arce, M Asai, T Aso, E Bagli, A Bagulya, S Banerjee, G Barrand, et al. Recent developments in geant4. *Nuclear Instruments and Methods in Physics Research Section A: Accelerators, Spectrometers, Detectors and Associated Equipment*, **835**:186–225, 2016.

Loïc Grevillot, Thibault Frisson, Nabil Zahra, Damien Bertrand, Frédéric Stichelbaut, Nicolas Freud, and David Sarrut. Optimization of GEANT4 settings for proton pencil beam scanning simulations using GATE. *Nuclear Instruments and Methods in Physics Research Section B: Beam interactions with materials and atoms*, **268**(20):3295–3305, 2010.

ICRU. report 90. key data for ionizing-radiation dosimetry: Measurement standards and applications. Journal of the ICRU, **14**(1), 2014.

Anton V Ivantchenko, Vladimir N Ivanchenko, Jose-Manuel Quesada Molina, and Sebastien L Incerti. Geant4 hadronic physics for space radiation environment. *International journal of radiation biology*, **88**(1-2):171–175, 2012.

Carlino A, Stock M, Zagler N, Marrale M, Osorio J, Vatnitsky S, Palmans H. Characterization of PTW-31015 PinPoint ionization chambers in photon and proton beams. *Physics in Medicine & Biology*, **63**(18):185020, 2018

Hermann Fuchs, Stanislav Vatnitsky, Markus Stock, Dietmar Georg, and Loïc Grevillot. Evaluation of GATE/Geant4 multiple Coulomb scattering algorithms for a 160MeV proton beam. *Nuclear Instruments and Methods in Physics Research Section B: Beam Interactions with Materials and Atoms*, 410:122–126, 2017.

RF Laitano and M Rosetti. Proton stopping powers averaged over beam energy spectra. *Physics in medicine and biology*, **45**(10):3025, 2000.

Carles Gomà, Pedro Andreo, and Josep Sempau. Monte carlo calculation of beam quality correction factors in proton beams using detailed simulation of ionization chambers. *Physics in Medicine & Biology*, **61**(6):2389, 2016.

Andreas F Resch, Alessio Elia, Hermann Fuchs, Antonio Carlino, Hugo Palmans, Markus Stock, Dietmar Georg, and Loïc Grevillot. Evaluation of electromagnetic and nuclear scattering models in gate/geant4 for proton therapy. *Medical physics*, **46**(5):2444–2456, 2019.

Table

Click here to download high resolution image

Purpose	Measurement description	Measured quantity	Measured data set
Beam optics modeling	spot map	Source Axes Distance, FWHM in air	20 energies per 7 air gaps
Energy spectra modeling	depth dose profile for a pristine Bragg curve	range in water, integrated depth dose profile	20 energies at isocenter
Beam optics residual evaluation with RaShi	spot map	FWHM in air	4 energies, 5 air gaps, with RaShi
Depth dose residual evaluation with RaShi	depth dose profile single spot	range in water, integrated depth dose profile	4 energies measured at non-isocentric position with RaShi
Beam model dose calibration and residual evaluation in 2D	dose in reference condition for scanned fields	Dose Area Product	9 energies
Beam model final validation in 3D	3D dose distribution in water	field size, lateral penumbra, modulation, dose	3 boxes measured at isocenter, 1 non-isocentric box with RaShi, 7 clinical plans in non-isocentric conditions with or without RaShi

Table

Click here to download high resolution image

z_{ref} [cm]	Nominal energy [MeV/n]	Monte Carlo $d_w(S^{\rho}_{el}, \Phi^{A}_{z})$ [MeV cm^2 g^{-1}]	R80 [cm]	Rp [cm]	R80-z_{ref} [cm]	ICRU90 $(S/\rho)_w(E_i, z_{ref})$ [MeV cm^2 g^{-1}]	relative difference to ICRU90 [%]
1.4	62.4	14.48	2.98	3.11	1.58	14.42	0.39%
1.4	72.4	11.80	3.98	4.12	2.58	11.63	1.47%
1.4	81.3	10.29	4.98	5.12	3.58	10.08	2.13%
1.4	97.4	8.55	6.98	7.14	5.58	8.34	2.57%
2.0	97.4	8.99	6.98	7.14	4.98	8.75	2.71%
2.0	111.6	7.86	8.97	9.18	6.97	7.59	3.64%
2.0	124.7	7.12	10.99	11.23	8.99	6.82	4.30%
2.0	136.8	6.60	12.99	13.27	10.99	6.28	5.35%
2.0	148.2	6.21	15.00	15.31	13.00	5.86	5.78%
2.0	159.0	5.88	17.00	17.34	15.00	5.54	6.30%
2.0	169.3	5.64	19.00	19.39	17.00	5.27	7.10%
2.0	179.2	5.42	21.00	21.41	19.00	5.04	7.43%
2.0	188.7	5.23	22.98	23.42	20.98	4.85	7.79%
2.0	198.0	5.07	24.99	25.46	22.99	4.68	8.18%
2.0	207.0	4.93	26.99	27.49	24.99	4.54	8.50%
2.0	215.7	4.81	28.97	29.51	26.97	4.41	8.97%
2.0	224.2	4.69	30.96	31.53	28.96	4.29	9.28%
2.0	232.6	4.58	32.97	33.58	30.97	4.19	9.34%
2.0	240.8	4.50	35.00	35.64	33.00	4.09	10.07%
2.0	248.8	4.41	36.99	37.66	34.99	4.01	10.09%
2.0	252.7	4.37	38.08	38.68	36.08	3.96	10.36%

Table

Click here to download high resolution image

Box type	FS50 [mm]	LP80-20- [mm]	LP80-20+ [mm]
Box6(0,0,6)	0.3 (0.4%)	-1.0 (-11.4%)	0.0 (0.1%)
Box8(0,0,15)	0.3 (0.3%)	-0.2 (-2.4%)	-0.2 (-2.0%)
Box10(0,0,25)	0.1 (0.1%)	0.3 (1.1%)	0.2 (2.1%)
Box6(0,0,5) ISD-50cm+RaShi	1.0 (1.2%)	-0.4 (10.3%)	0.2 (-2.4%)

Box type	R80 [mm] (%)	R90 [mm] (%)	Rp [mm] (%)	MOD90 [mm] (%)	DP80-20 [mm] (%)
Box6(0,0,6)	0.0 (0.0%)	0.1 (0.0%)	-0.7 (-0.7%)	-1.0 (-1.5%)	-0.6 (-24.7%)
Box8(0,0,15)	0.0 (0.0%)	0.0 (0.0%)	-0.4 (-0.2%)	1.3 (1.4%)	-0.5 (-14.0%)
Box10(0,0,25)	-0.1 (0.0%)	-0.2 (-0.1%)	-0.4 (-0.1%)	2.1 (1.7%)	-0.5 (-9.0%)
Box6(0,0,5) ISD-50cm+RaShi	0.5 (0.6%)	0.7 (0.9%)	-0.2 (-0.2%)	0.8 (1.3%)	-0.5 (-16.0%)

Figure

Click here to download high resolution image

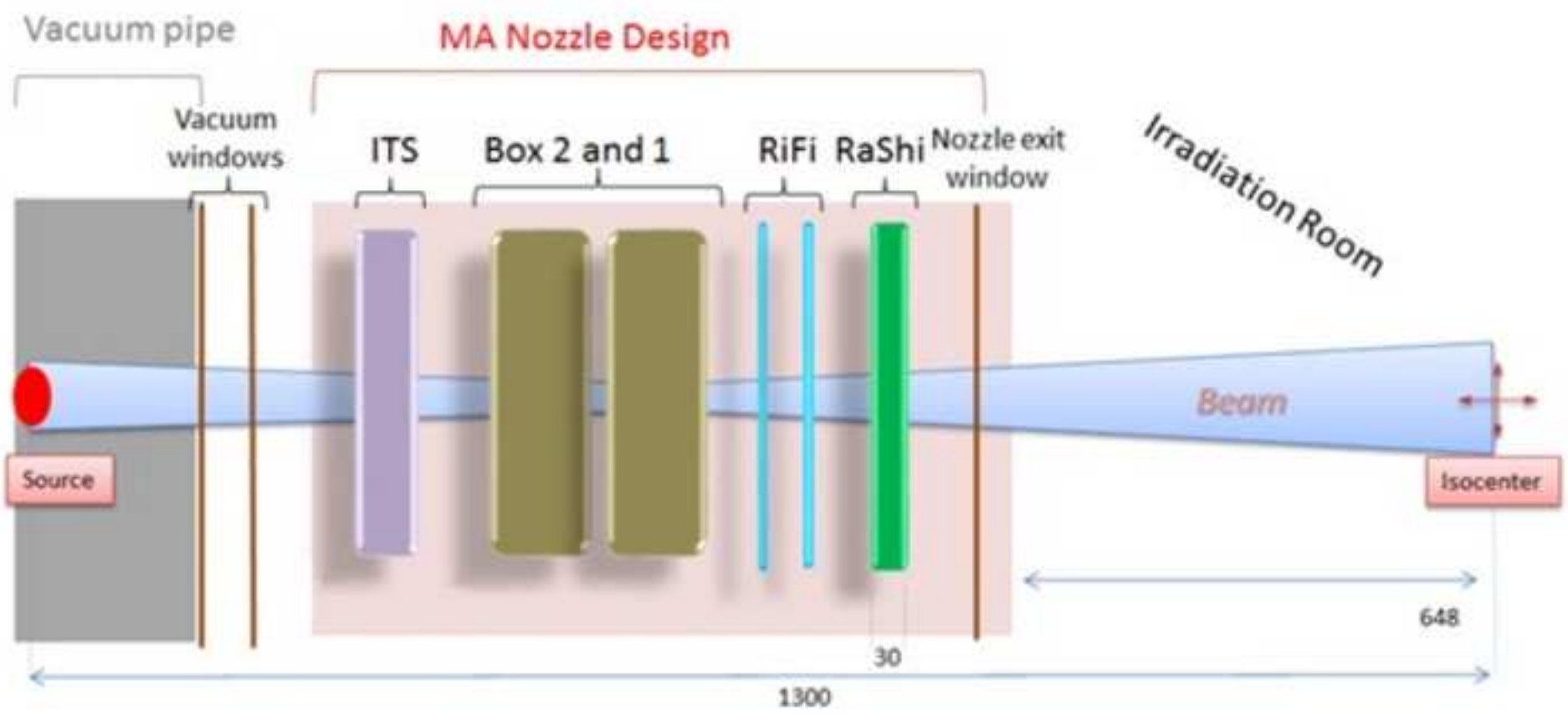

Figure
Click here to download high resolution image

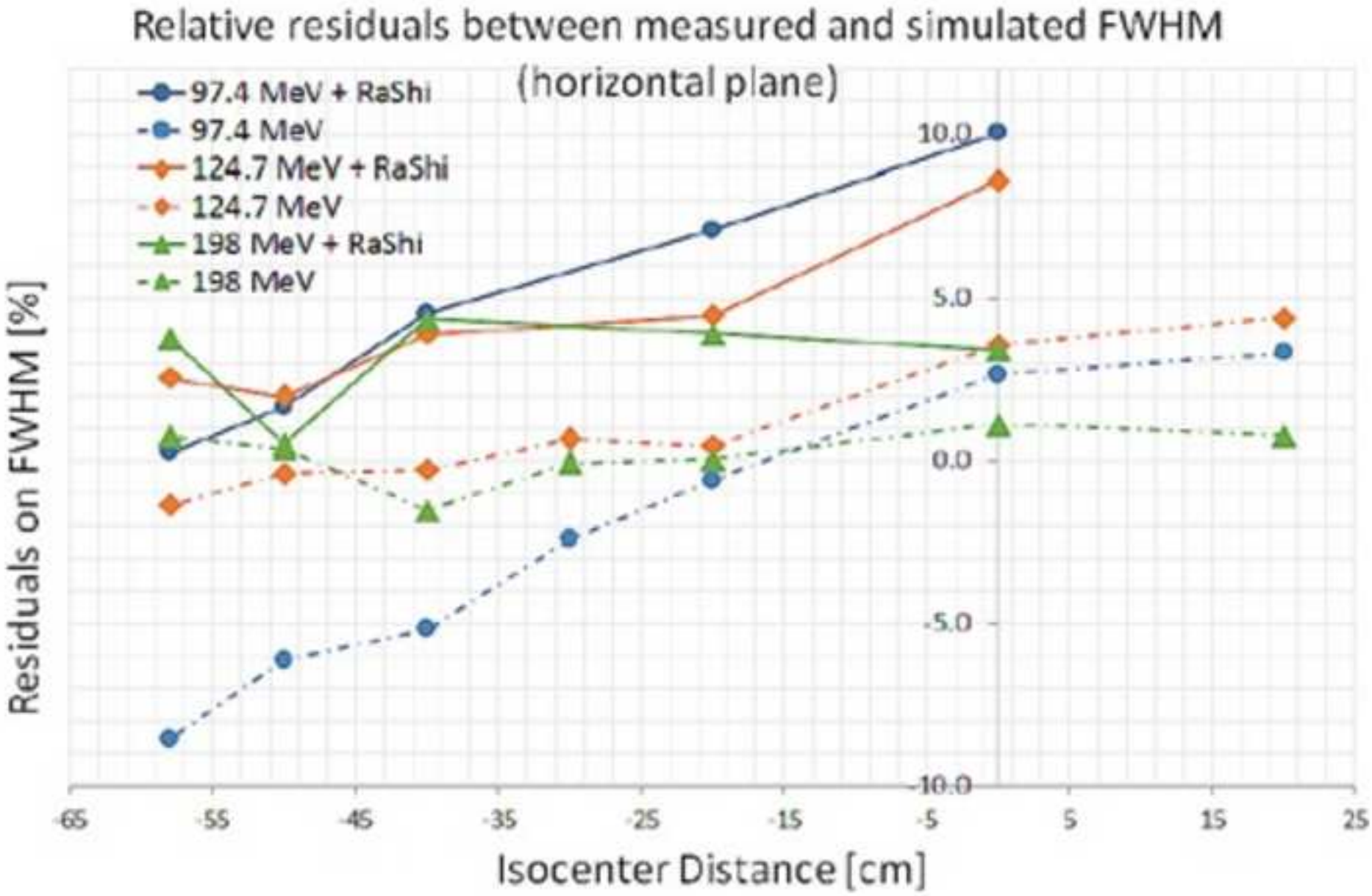

Figure

Click here to download high resolution image

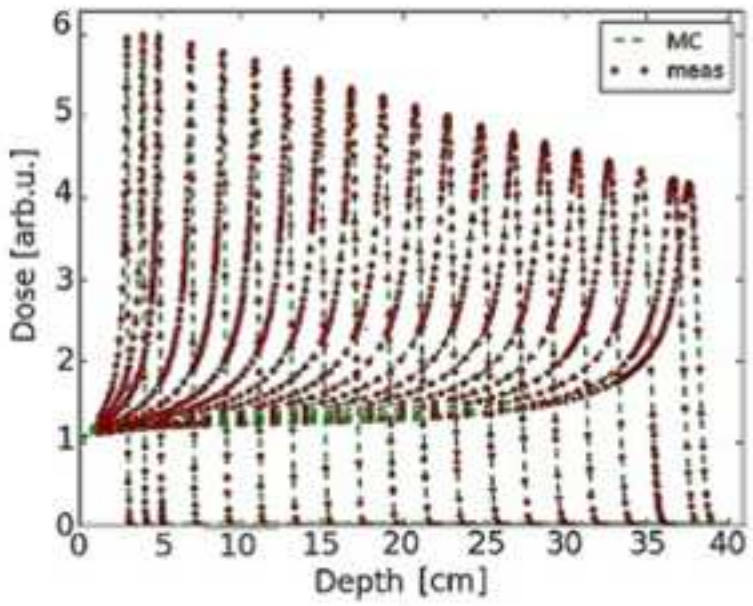

(a)

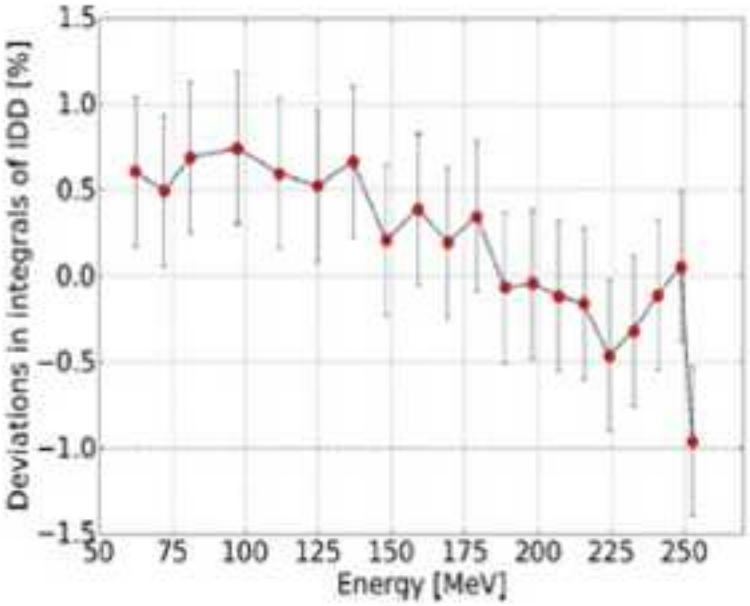

(b)

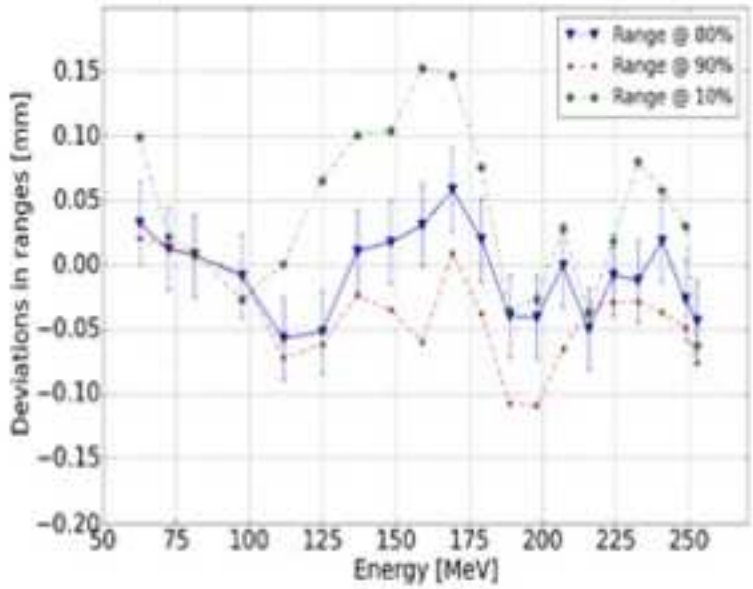

(c)

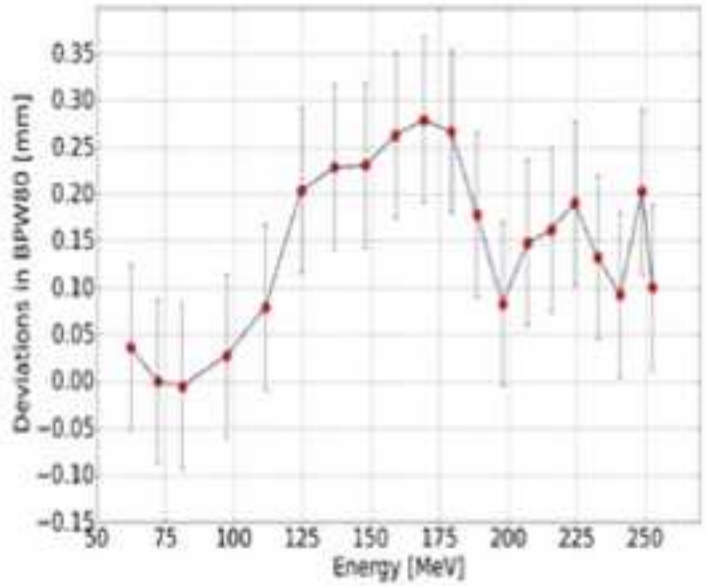

(d)

Figure

Click here to download high resolution image

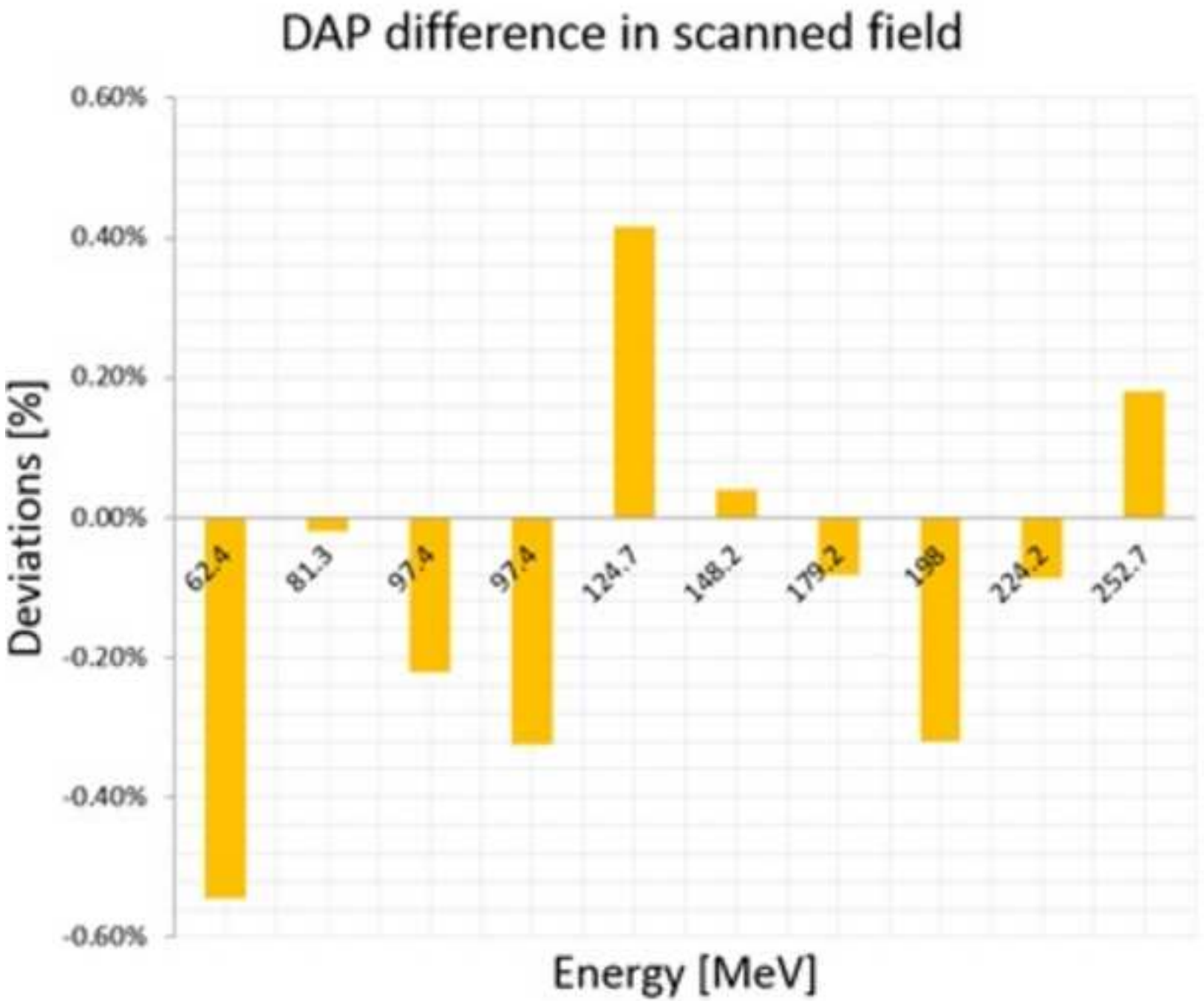

Figure
Click here to download high resolution image

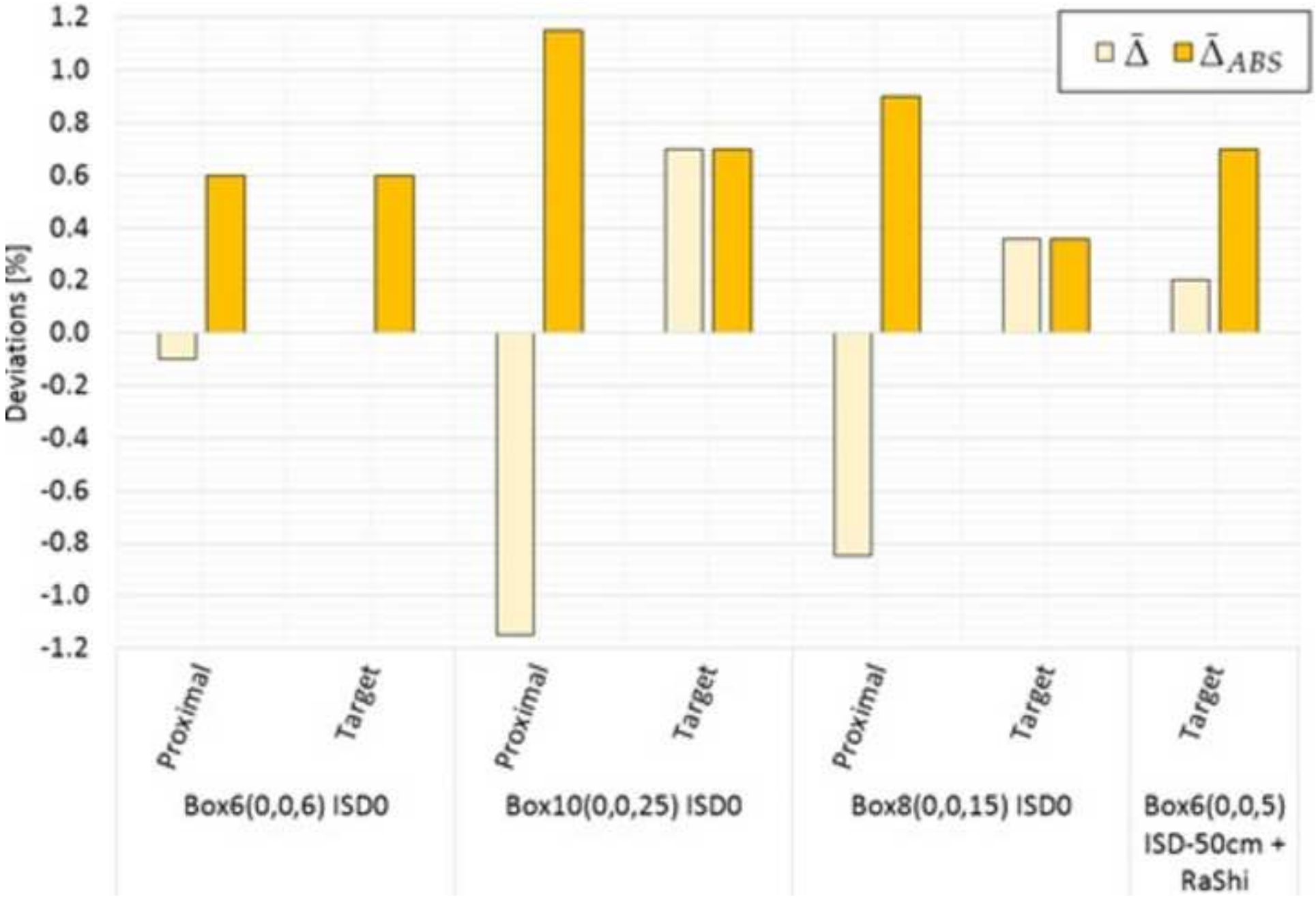

Figure

Click here to download high resolution image

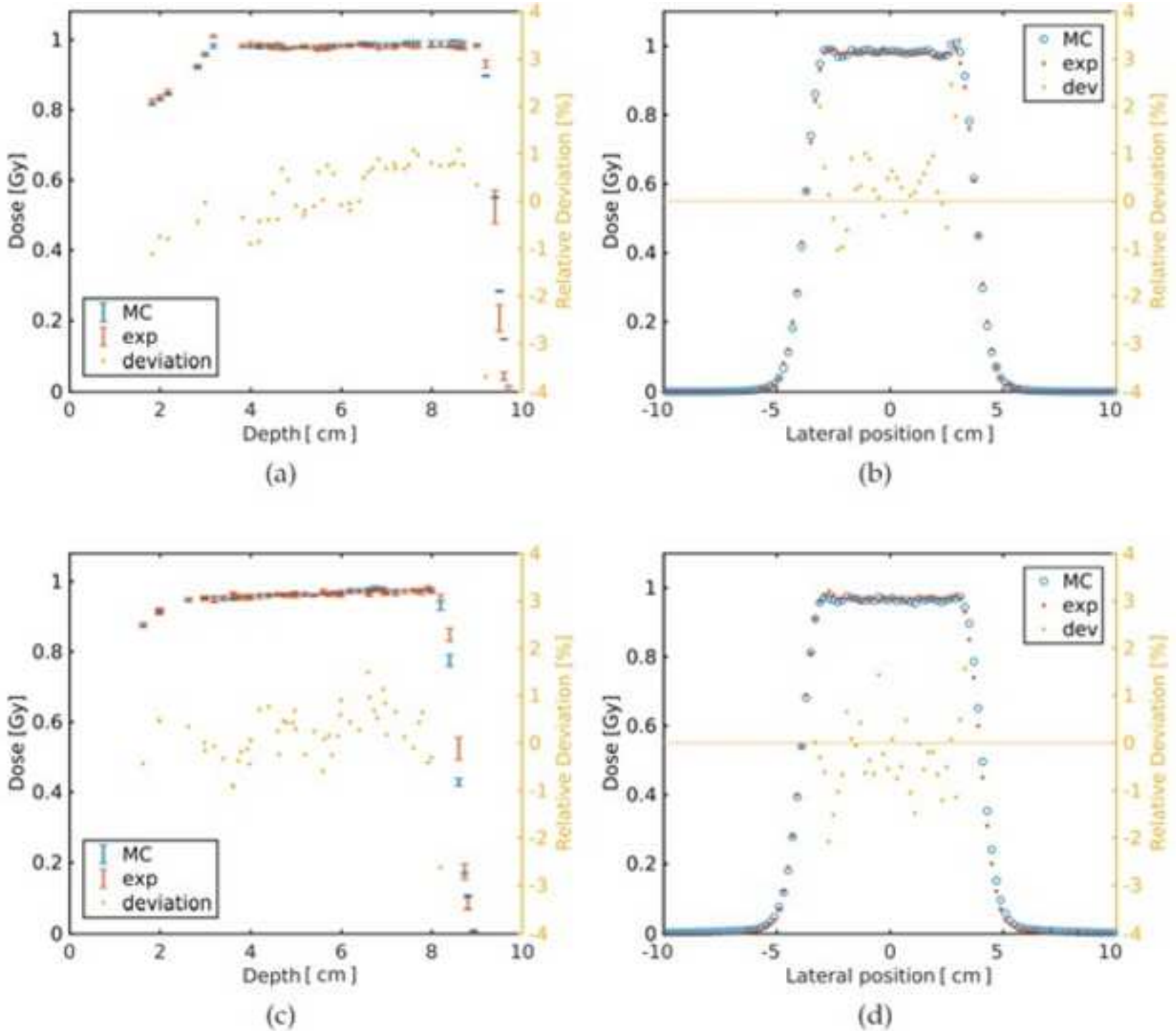

Figure

Click here to download high resolution image

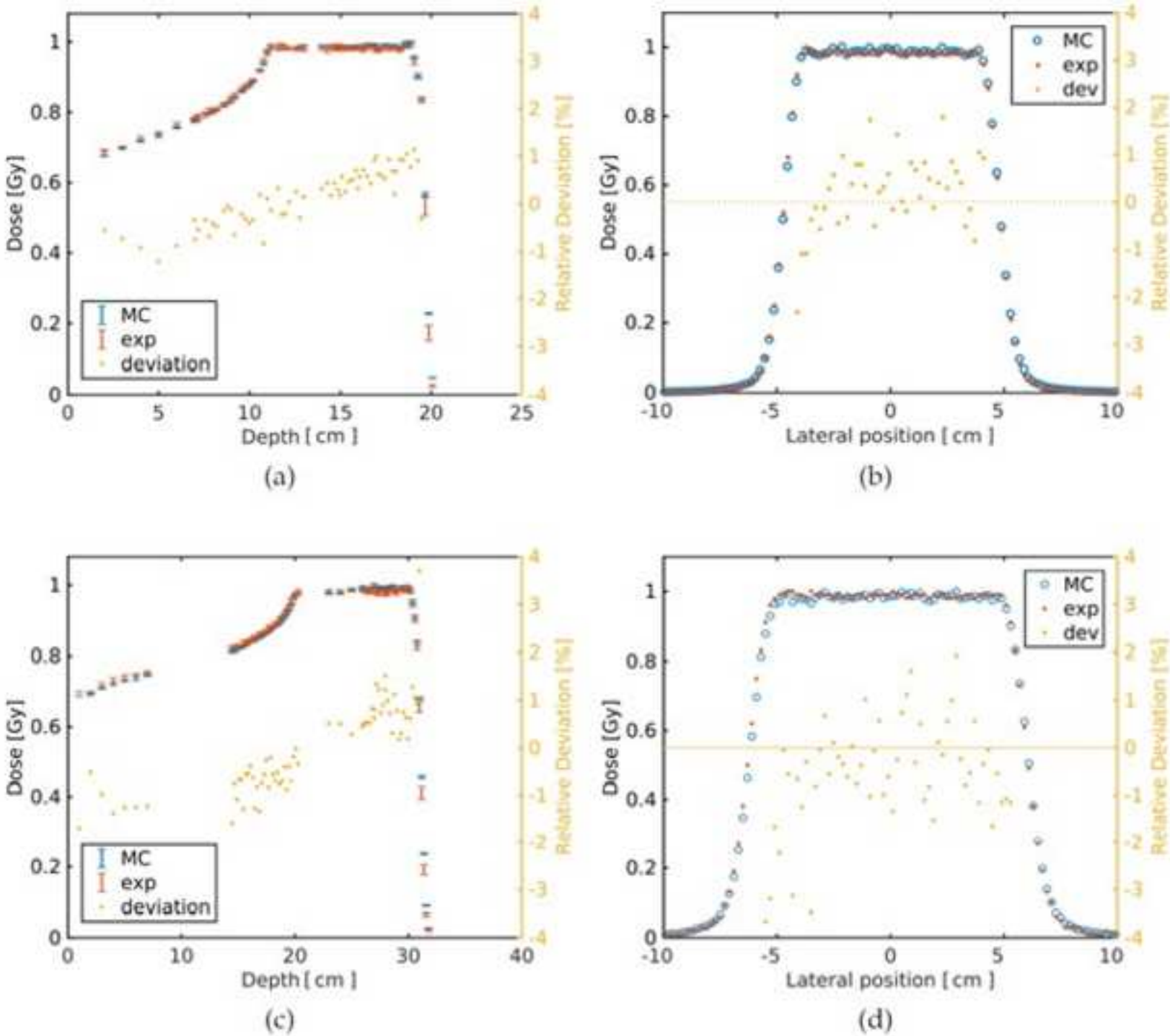

Figure
Click here to download high resolution image